Bioelectrochemistry 149 (2023) 108301

Contents lists available at ScienceDirect

Bioelectrochemistry

journal homepage: www.journals.elsevier.com/bioelectrochemistry

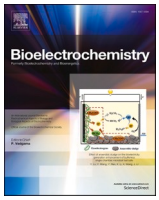

Co phthalocyanine mediated electrochemical detection of the HER2 in the presence of Au and CeO_2 nanoparticles and graphene quantum dots

Sixolile Centane, Tebello Nyokong *

Institute of Nanotechnology Innovation, Rhodes University, Makhanda 6140, South Africa

ARTICLE INFO

Keywords:
Nanomaterial based biosensor
Human epidermal growth factor (HER2)
Electrochemical Impedance Spectroscopy
Gold nanoparticles
Cobalt Phthalocyanines

ABSTRACT

In this work, cobalt tetra phenoxy acetic acid phthalocyanine (CoTAPc) is investigated as an electron mediator, immobilization platform for an HB5 aptamer and to enhance the electrochemical signal for the detection of human epidermal growth factor receptor 2 (HER2). Furthermore, the CoTAPc was combined individually with sulphur/nitrogen doped graphene quantum dots (SNGQDs), gold nanoparticles (AuNPs) and cerium oxide nanoparticles (CeO_2NPs), on a glassy carbon electrode (GCE) via sequential adsorption. The CoTAPc and SNGQDs were also π-π stacked, used for electrode modification similarly to the rest of the other surfaces and applied towards the electrochemical detection of HER2. The designed sensors were characterized using electrochemical impedance spectroscopy (EIS). The designed aptasensors showed detection limits as low as 6.0 pg/mL. The real life applicability of the designed aptasensors was tested in human serum samples. The aptasensors showed great storage stability, sensitivity and specificity towards HER2, implying great potential for applications in early diagnosis of breast cancer.

1. Introduction

An electrochemical biosensor can be defined as an analytical device which converts a biological response into a quantifiable and processable signal via electrochemical transduction [1]. In an electrochemical biosensor, the signal transduction and the general performance are determined by the surface architectures that connect the sensing element to the biological sample [2,3]. Surface architecture development involves modification of an electrode to achieve immobilization of biomolecules, for signal amplification and measurement [4,5]. In this work we compare the efficiency of cerium oxide nanoparticles (CeO_2NPs), gold nanoparticles (AuNPs), and sulfur-nitrogen doped graphene quantum dots (SNGQDs) in enhancing the electrocatalytic activity of a cobalt tetraphenoxy acetic acid phthalocyanine (CoTAPc) towards the electrochemical detection of the human epidermal growth factor receptor 2 (HER2) in the presence of an aptamer. An HB5 DNA aptamer is HER2 specific and hence is the biorecognition element of interest in this work. HER2 is an established breast cancer biomarker, and is often overexpressed in breast cancer. HER2 plays a role in increasing proliferation and survival of the primary tumour as well as metastases [6,7]. Combining a Pc with nanoparticles (NPs) is expected to enhance the HER2 sensing signal by synergistic effect. This means that if we combine the electrocatalytic properties Pcs possess with the good conducting properties of NPs, we can expect a better signal than using them separately, and thus will contribute further to signal amplification of the aptasensor. Phthalocyanines are 18 π-electron macrocyclic compounds, with high thermal stability and redox activity [8]. In the design of biosensors, phthalocyanines have been used as electron transfer mediators as well as to enhance the electro-catalytic activity of the redox processes [9]. A CoPc derivative is employed together with these NPs since they are well known electrocatalysts [10].

As stated above the employed NPs are: AuNPs, CeO_2NPs and SNGQDs. Gold nanoparticles are the most commonly used nanomaterial in the biosensor design. A major advantage of using AuNPs in biosensors is the increase in detection signal for analytes at low concentrations [11,12]. GQDs are made of a single layer of sp^2 carbon bond atoms that are arranged in a 2D lattice and are known for their conductivity and high surface area [13]. These characteristics allow rapid electron transfer for the detection of biomolecules. Doping of graphitic materials with hetero atoms is known to improve electrocatalytic activity [14] hence S and N doped GQDs are employed in this work. Cerium oxide nanoparticles (CeO_2NPs) contain intriguing catalytic and electrochemical properties due to their unique chemical and electronic configurations, mechanical stability, and biocompatibility [15–17].

* Corresponding author.
E-mail address: T.nyokong@ru.ac.za (T. Nyokong).

https://doi.org/10.1016/j.bioelechem.2022.108301
Received 17 August 2022; Received in revised form 3 October 2022; Accepted 8 October 2022
Available online 15 October 2022

AuNPs have been employed in the presence of porphyrinoids and aptamer for biosensing of prostate specific antigen or HER2 [18,19]. We have reported on the use of a cobalt tetra phenoxy carboxy phthalocyanine in the presence of graphene quantum dots towards the detection of HER2 [20]. We have also reported on the use of a cobalt tetra phenoxy acetic acid phthalocyanine (CoTAPc, Fig. 1) in the presence of cerium oxide nanoparticles towards the detection of HER2 [21]. CoTAPc is employed for the first time in the presence of three different types of nanoparticles: carbon based (SNGQDs), metallic (AuNPs) and metal oxide (CeO_2 NPs). This is also the first time that a Pc is studied for HER2 detection in the presence of AuNPs. Both SNGQDs and CoTAPc contain π electrons and can interact with each other through π-π stacking forming SNGQDs(π)CoTAPc. Thus we compare the performance of SNGQDs(π) CoTAPc as compared to their sequential addition to the electrode in SNGQDs/CoTAPc(seq.). The nanoparticles and CoTAPc contain carboxylic groups to allow for the covalent immobilization of the amino functionalized HB5 aptamer on the electrode surface. We examine the effect of the nature of the nanoparticle on the sensing ability of CoTAPc, bearing in mind that size and defects of the nanoparticle affect the conducting abilities.

2. Experimental

2.1. Materials

The following materials were purchased from Sigma Aldrich: human serum, bovine serum albumin (BSA), *N*-hydroxy succinimide (NHS), diethylamine (DEA), acetic acid, 1,3-dicyclohexylcarbodiimide (DCC), Na_2HPO_4, KH_2PO_4, NaCl, KCl, $K_4[Fe(CN)_6]$, $K_3[Fe(CN)_6]$, and the protein (human epidermal growth factor receptor 2, HER2). The HB5 DNA aptamer (5′−/5 Am MC6/AAC CGC CCA AAT CCC TAA GAG TCT GCA CTT GTC ATT TTG TAT ATG TAT TTG GTT TTT GGC TCT CAC AGA CAC ACT ACA CAC GCA CA-3′) was purchased from Integrated DNA technologies (IDT), South Africa. Phosphate buffer saline (PBS, pH 7.4) was prepared using weighed amounts of Na_2HPO_4, KH_2PO_4, KCl and NaCl. Millipore water was obtained from Type II water from an Elga PURELAB Chorus 2 (RO/DI) system. The HB5 DNA aptamer was prepared according to the manufacturer's instructions for 100 μM in 10 mM PBS of pH 7.4. HER2 protein (specific target) was sold as a solution, with concentration of 4.4 mg/mL: necessary dilutions were prepared using PBS (pH 7.4). 1 % BSA for non-specific binding was prepared using PBS solution (pH 7.4). All stock solutions were prepared using Millipore water and were kept at 20 °C during the course of the study. The CoTAPc, CeO_2NPs (containing COOH) [21] and AuNPs (capped with oleylamine) [22] and SNGQDs (containing COOH) [19,23] were all synthesized following reported literature methods.

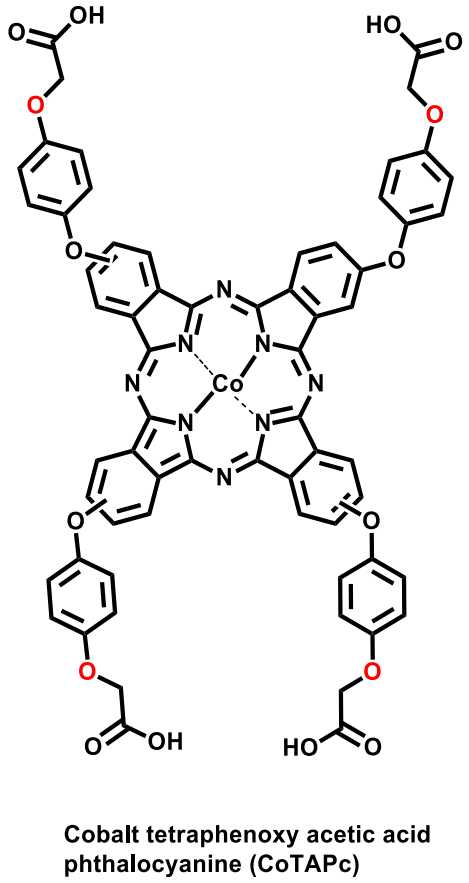

Fig. 1. The structure of the cobalt phthalocyanine (CoTAPc).

2.2. Equipment

Electrochemical impedance spectroscopy (EIS) and cyclic voltammetry (CV) studies were performed using an Autolab Potentiostat PGSTAT30 equipped with Nova software version 2.1. The EIS experiments were performed between 0.1 and 100000 Hz, using 0.01 V_{RMS} sinusoidal modulation. A non-linear least squares (NLLS) method based on the EQUIVCRT programme was used for automatic fitting of the obtained EIS data. A Bruker Vertex 70-Ram II Raman spectrometer (equipped with a 1064 nm Nd: YAG laser and liquid nitrogen cooled germanium detector) was used to collect Raman data. Infrared spectra were recorded on a Bruker® Alpha IR (100 FT-IR) spectrophotometer. Ground state electronic absorption spectra were performed on a Shimadzu UV-2550 spectrophotometer. X-ray powder diffraction (XRD) patterns were recorded on a Bruker D8 Discover equipped with a Lynx-Eye Detector, using CuKα radiation (=1.5405 Å, nickel filter).

2.3. π-π stacking of CoTAPc onto SNGQDs

The SNGQDs are sp^2 hybridized and are highly π - conjugated type of nanomaterials which can undergo π-π interactions with any similarly conjugated nanomaterials. Phthalocyanines being π-electron rich, qualify for π-π stacking with the SNGQDs and this was done as follows: SNGQDs (5 mL, 1 mg/mL) were added to a CoTAPc solution (5 mL, 8.086×10^{-4} mmol in DMSO), followed by stirring to mix the two. Following that, the mixture was sonicated for 4 h to give SNGQDs(π) CoTAPc.

2.4. Electrode modification

All the solutions were freshly prepared in Milli-Q water and stored at the temperature of 4 °C until use. Solutions were deaerated by bubbling argon gas prior to the electrochemistry experiments and the electrochemical cell was kept under argon atmosphere throughout the experiments. Glassy carbon electrodes were first polished with Al_2O_3 powder (Aldrich, 0.1, 0.05 mm) using Metrohm polishing kit, and rinsed with deionized water, followed by sonication in ethanol and deionized water. Finally, the electrodes were allowed to dry at room temperature. The glassy carbon electrodes (GCEs) were modified by the drop dry method where the modifier was dropped on the electrode followed by drying as follows: the freshly cleaned GCE was modified using 10 μL (of 1 mg/mL in water, except for CoTAPc which was in DMSO) each of CoTAPc, SNGQDs, CeO_2NPs, AuNPs and SNGQDs(π)CoTAPc, to form the electrodes: GCE/CoTAPc(**1**), GCE/SNGQDs(**2**), GCE/CeO_2NPs(**3**), GCE/AuNPs(**4**) and GCE/SNGQDs(π)CoTAPc(**5**). respectively. The electrodes were dried in the oven at 70 °C. Experiments were also performed where GCE was modified by sequential addition whereof the various nanoparticles followed by addition of CoTAPc, using the same amounts stated above. We have shown that the best catalytic activity is obtained when MPcs are placed on top of nanomaterials [24], hence in this work for the

sequentially modified electrodes, NPs are placed first on the electrode followed by CoTAPc. The sequentially modified electrodes are as follows: GCE/SNGQDs/CoTAPc(seq)(**6**), GCE/CeO_2NPs/CoTAPc(**7**), and GCE/AuNPs/CoTAPc(**8**). Please note that in order to differentiate from GCE/SNGQDs(π)CoTAPc(**5**), the electrode modified sequentially (seq) with SNGQDs and CoTAPc is represented as GCE/SNGQDs/CoTAPc(seq)(**6**). The total list of electrodes is shown in Table 1.

2.5. Fabrication of biosensor

The recognition element of choice in this work is the HB5 aptamer, with an amino functionalized terminal. SNGQDs, CeO_2NPs, and CoTAPc contain carboxylic acid groups. The immobilization of the HB5 on the surface modified GCE is by means of an amide linkage bond using DCC/NHS coupling, for all electrodes containing COOH groups (Scheme 1). This excludes the GCE/AuNPs probe where the AuNPs were capped with oleylamine. For AuNPs, the loosely bound oleylamine will be replaced by HB5 through the binding of the NH_2 groups of the latter with Au.

A total of 8 electrodes: GCE/CoTAPc(**1**), GCE/SNGQDs(**2**), GCE/CeO_2NPs(**3**), GCE/AuNPs(**4**), GCE/SNGQDs(π)CoTAPc(**5**), GCE/SNGQDs/CoTAPc(seq.)(**6**), GCE/CeO_2NPs/CoTAPc(**7**), GCE/AuNPs/CoTAPc(**8**), were studied for sensor development towards the electrochemical detection of HER2. To all the modified surfaces (except for GCE/AuNPs(**4**)), DCC (6.0 mg, 0.029 mmol) and NHS (4.0 mg, 0.035 mmol) were added, the electrodes were left at room temperature for 1 h. The HB5 aptamer (10 μL, 1.0 μM) was then dropped on the DCC/NHS activated surfaces giving : GCE/CoTAPc(**1**)/HB5, GCE/SNGQDs(**2**)/HB5, GCE/CeO_2NPs(**3**)/HB5, GCE/SNGQDs(π)CoTAPc(**5**)/HB5, GCE/SNGQDs/CoTAPc(seq.)(**6**)/HB5, GCE/CeO_2NPs/CoTAPc(**7**)/HB5, and GCE/AuNPs/CoTAPc(**8**)/HB5. The procedure for the formation GCE/AuNPs(**4**)/HB5 was done following a ligand approach method reported in [25–27]: the HB5 aptamer (10 μL, 1.0 μM) was placed on the GCE/AuNPs to allow the *N*-Au bond to form. The GCE/AuNPs was first immersed in 500 μL of diethylamine (DEA) solution for 1 h, to displace and replace the oleylamine ligand on the AuNPs surface. The DEA was then removed by rinsing the electrode surface with dilute acetic acid. DEA is a small amine molecule, which can be conveniently removed from the metal surface by protonation with an acid [26]. Following that, 10 μL of the HB5 solution was added onto the GCE/AuNPs to form the GCE/AuNPs/HB5 surface.

All eight electrodes were then treated with 1 % BSA (bovine serum albumin) to prevent non-specific binding, and again rinsed with PBS. The electrochemical response of the electrodes in the presence of varying concentrations of the HER2 antigen was measured using the electrochemical impedance spectroscopy (EIS). The EIS measurement was conducted under the stable open circuit potential with the frequency varying from 0.1 to 100000 Hz, using 0.01 V_{RMS} sinusoidal modulation.

2.6. HER2 detection in human serum

Preliminary experiments for the determination of HER2 protein in human serum samples were also performed. The designed aptasensors were tested in 1/500 diluted (in 0.1 M PBS buffer, pH 7.4) serum samples spiked with standard addition of HER2 protein (3 ng/mL, 5 ng/mL, 7 ng/mL and 9 ng/mL). The response of the aptasensors was then determined by EIS measurements, under the same conditions used for HER2 calibration curve.

Table 1
Peak potential separations and R_{ct} values in $[Fe(CN)_6]^{3-/4-}$ of all the modified electrodes prior to HB5 immobilization.

Modified Electrode*	ΔEp (mV)	Rct (Ω)	Γ, mol cm^{-2}
GCE/CoTAPc(**1**)	71	1520	1.11×10^{-14}
GCE/SNGQDs(**2**)	75	1580	No peak
GCE/CeO_2NPs(**3**)	122	1750	4.49×10^{-9}
GCE/AuNPs(**4**)	100	1680	1.82×10^{-7}
GCE/SNGQDs(π)CoTAPc(**5**)	80	1600	1.49×10^{-13}
GCE/SNGQDs/CoTAPc(seq.)(**6**)	105	1700	9.76×10^{-10}
GCE/CeO_2NPs/CoTAPc(**7**)	70	827	2.65×10^{-10}
GCE/AuNPs/CoTAPc(**8**)	480	3900	3.99×10^{-9}

* Seq. = sequential adsorption modified.

2.7. Stability and repeatability

The reproducibility of the designed probes was investigated by running successive measurements at each HER2 concentrations in triplicate and the standard deviation was calculated. The relative standard deviation (RSD) was calculated for all eight electrodes at various concentrations and the values are shown in Table S1. The stability of the designed sensors was investigated using the shelf-life estimation method. Where, the sensors were stored at 4 °C over 96 h. The response of each probe was analyzed daily over the 96 hour period.

3. Results and discussions

3.1. Nanoparticle characterization

Fig. 2A shows the UV–vis spectra of the various synthesized materials. The UV–vis spectrum obtained for the AuNPs, Fig. 2A(i), is typical of gold nanospheres with an absorption peak at 599 nm. The SNGQDs, Fig. 2A (ii), had an absorption peak at 358 nm, which is typical of graphene quantum dots [19]. A broad peak was observed for the CeO_2NPs Fig. 2A (iii), at 339 nm. A typical phthalocyanine absorption spectrum was obtained for the CoTAPc (Fig. 2B(i)) with the: Q-band at 697 nm, and the Soret band at 331 nm. A similar spectrum was observed for SNGQDs(π)CoTAPc (Fig. 2B(ii)), with no significant shifts of the Q band, but broadened. An intensified and broadened Soret band with absorption maxima at 368 nm, which might be attributed to the presence of the SNGQDs in the sample. The spectrum of the conjugate exhibited characteristics of the individual components.

XRD was used to study the crystalline phase and components of the various samples, Fig. 3. For the SNGQDs sample, a typical XRD pattern for carbon based nanomaterials was observed, with the 002 peak at around $2\theta \sim 21^{\circ}$, Fig. 3. The diffractogram of the CeO_2NPs (Fig. 3), showed peaks with indices (111), (200), (220), (311), (222), (400), (331), and (420). Five diffraction peaks were observed for AuNPs (Fig. 3) which indexed to the (111), (200), (220), (311) and (222) reflections of face cantered cubic structure of metallic gold. The XRD pattern of the CoTAPc alone showed an amorphous peak at around $2\theta \sim 20^{\circ}$ (figure not shown). The XRD pattern of the SNGQDs(π)CoTAPc was similar to that of that SNGQDs, which is confirmation to that the structural integrity of the SNGQDs was preserved during conjugation. The various nanomaterial samples were also analysed using Raman Spectroscopy, Fig. 4. The reported [12] D and G bands for SNGQDs are at 1297 cm^{-1} and 1597 cm^{-1} with an intensity ratio I_D/I_G of 1.39. Upon conjugation of the SNGQDs to the CoTAPc via non-covalent π-interactions, Fig. 4, a minimal shift in the D (1299 cm^{-1}) and G (1600 cm^{-1}) bands, accompanied by an increase in the I_D/I_G ratio (1.44) was observed. The minimal shift in the D and G bands, might be due to the fact that non-covalent interactions allows for structural preservation of the involved nanostructures. The Raman data obtained for the CeO_2NPs alone is shown in Fig. 4: a first order Raman peak (F_{2g}) at 449 cm^{-1} and five second order Raman peaks prominent at 595 cm^{-1}, 823 cm^{-1}, 895 cm^{-1}, 989 cm^{-1} and 1051 cm^{-1} were observed [28,29]. The feature at 595 cm^{-1} can be attributed to originate from O^{2-} replacement of cerium (IV) atoms by cerium (III) atoms or impurity atoms in the bulk [29,30]. The features at 823 cm^{-1} and 895 cm^{-1} are attributed O—O stretching vibration of peroxides. The bands at 989 cm^{-1} and 1051 cm^{-1} are as a result of second order scattering, with the former emanating from the combination of the A_{1g}, E_g, and F_{2g} modes [31]. A typical Raman spectroscopy for AuNPs was obtained and is shown in Fig. 4, with peaks at 382 cm^{-1}, 521 cm^{-1}, 627 cm^{-1}, 792 cm^{-1}, 1008 cm^{-1}, 1207 cm^{-1},

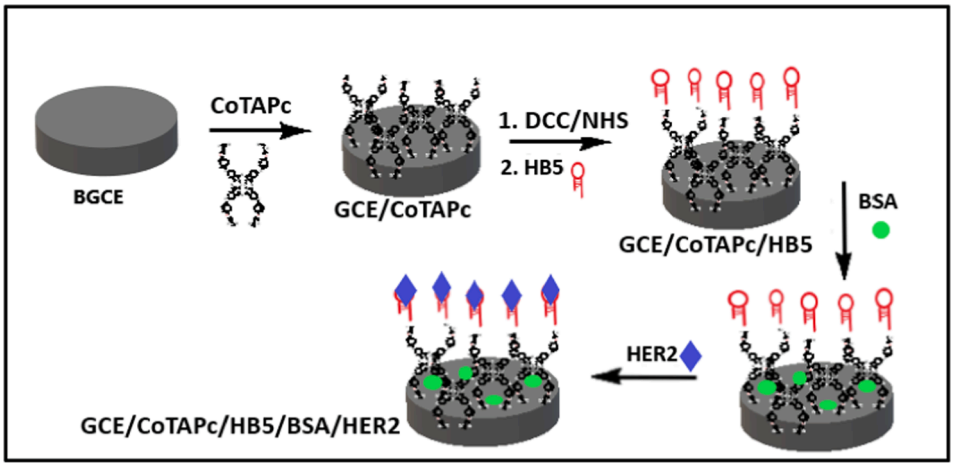

Scheme 1. Representation of the fabricated electrode.

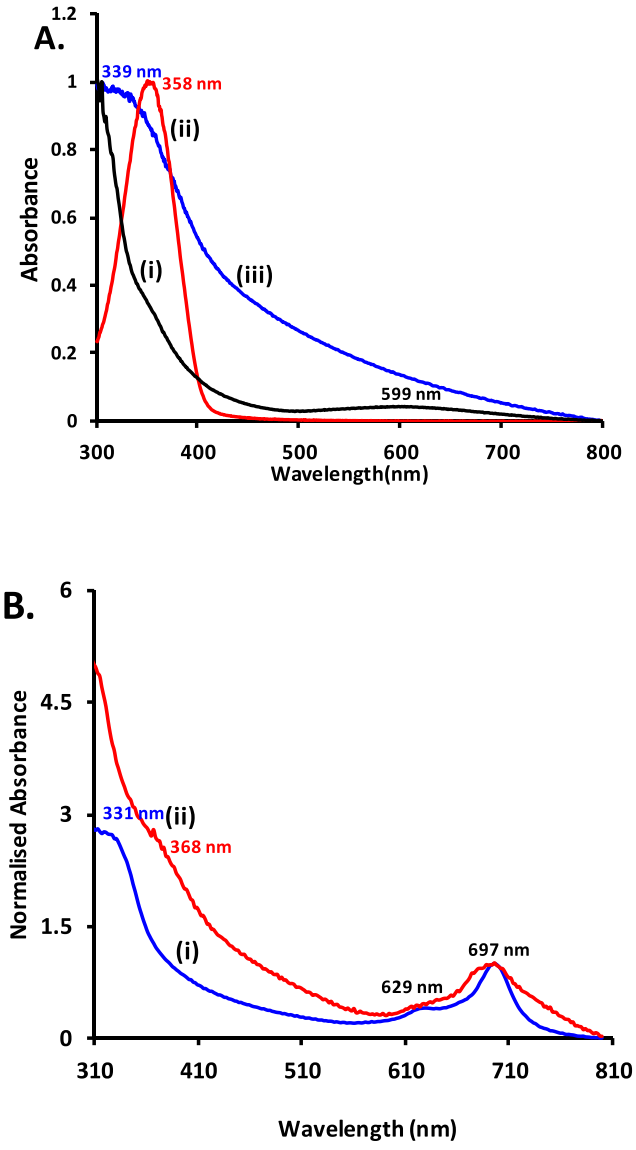

Fig. 2. UV–vis spectroscopy for (A) AuNPs (i), SNGQDs (ii), CeO_2NPs (iii) and (B) CoTAPc (i) and SNGQDs(π)CoTAPc (ii). The AuNPs were recorded in toluene, SNGQDs and CeO_2NPs in water while CoTAPc and SNGQDs(π)CoTAPc were recorded in DMF.

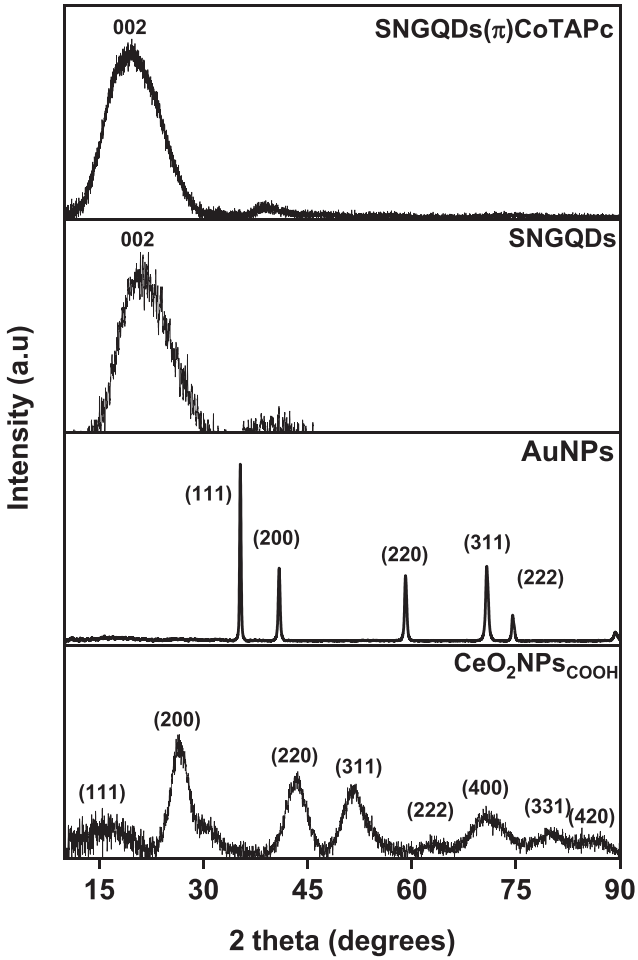

Fig. 3. XRD data obtained for the various nanoparticles as well as the nanoparticle-CoTAPc conjugates. Data labelled accordingly.

1215 cm^{-1}, 1383 cm^{-1} and 1608 cm^{-1}. The peaks observed are in good agreement with what has been reported in previous literature reports for gold nanoparticles [32,33].

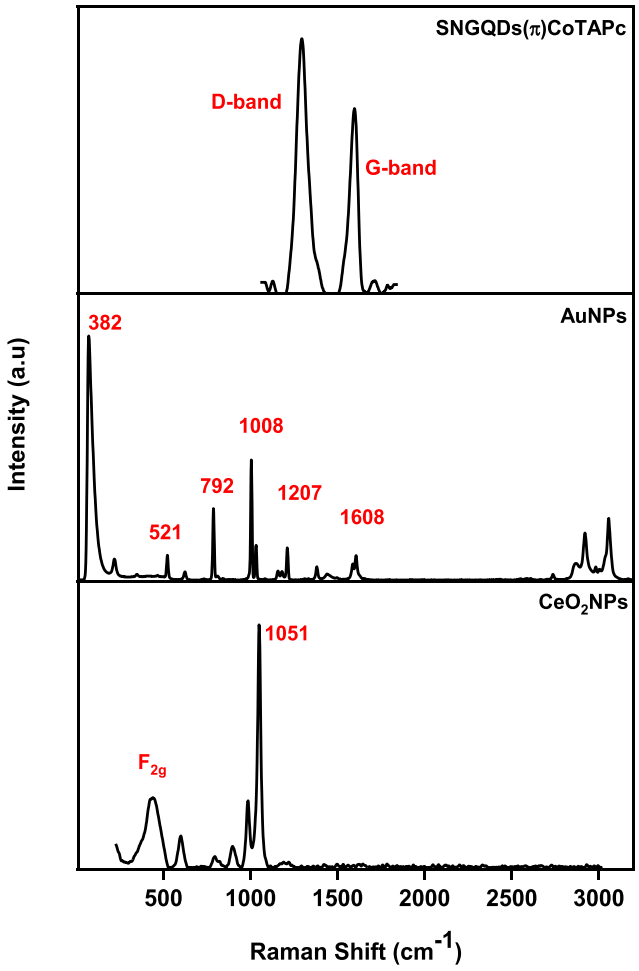

Fig. 4. Raman Spectroscopy of the SNGQDs(π)CoTAPc, AuNPs and CeO_2NPs.

3.2. Characterization of modified electrodes

3.2.1. Cyclic voltammetry

All electrochemical measurements were performed in 10 mM PBS of pH 7.4 containing 0.1 M KCl and 1 mM $[Fe(CN)_6]^{3-/4-}$, Fig. 5A. The CV of ferricyanide was chosen as a marker to investigate the electron transfer properties of each modified surface. The electron transfer properties of the various surfaces were investigated by comparing the ΔEp values (anodic to cathodic peak potential separation). A ΔE_p value close to or lower than ~ 70 mV is synonymous with desirable electron-transporting abilities. The calculated ΔEp values of 71 mV, 75 mV, 70 mV, and 80 mV for GCE/CoTAPc(**1**), GCE/SNGQDs(**2**), GCE/CeO_2NPs/CoTAPc(**7**), GCE/SNGQDs(π)CoTAPc(**5**), respectively, thus showing good electron-transporting abilities. The rest of the electrodes had ΔE_p value as follows: GCE/AuNPs/CoTAPc(**8**) (480 mV) > GCE/CeO_2NPs(**3**) (122 mV) > GCE/SNGQDs/CoTAPc (seq.)(**6**) (105 mV) > GCE/AuNPs(**4**) (100 mV). Of the NPs alone the lowest ΔE_p value was obtained for SNGQDs followed by AuNPs, with CeO_2NPs having the larges ΔE_p value. The varying performance of the various nanoparticles in the same redox media can be attributed to their different structural and physicochemical attributes. The process of electron transfer in nanoparticles can be explained considering the following factors. First, the contact between the electrode and the particular nanoparticle. This is determined by the spatial distribution of the nanoparticles on the electrode, which is dependent on the dispersion and behaviour of the nanoparticles in question when in solvent. Secondly, the nanoparticle's chemical nature, shape and size which determines how the nanoparticle interacts with the electrolyte as well as its stability on the electrode. The sheet structure of the SNGQDs allows for the successful deposition of the nanomaterials on the electrode, forming stable modified electrode. The SNGQDs were monodispersed with a size of 2.8 nm, as shown by TEM image in Fig. S1a. A high catalytic activity is generally expected for small particle size because of the increase of the surface-to-volume ratio [34]. In addition, spherical NPs are known to show better electrocatalytic activity than shaped ones, hence good charge transfer abilities and a low ΔE_p value for SNGQDs. The AuNPs used in this work were monodispersed with a spherical morphology, Fig. S1c.

The electron transfer properties of cerium oxide nanoparticles (CeO_2NPs) are derived from the quick and expedient mutation of the oxidation state between Ce^{4+} and Ce^{3+}. The morphology of the nanoparticles was confirmed as cubic shaped and were monodispersed. As reported before the COOH containing CeO_2NPs exhibited a rod like shape, Fig. S1b [21]. Hence the shape of the CeO_2NPs could have resulted in poor electron transfer (higher ΔE_p value) compared to SNGQDs and AuNPs. ΔE_p values for CoTAPc increase in the presejnce of SNGQDs and AuNPs, but is unaffected when CeO_2NPs are combined CoTAPc, Table 1. Thus the combination of CeO_2NPs and CoTAPc seems to improve charge transfer. Surprisingly for the GCE/AuNPs/CoTAPc, higher ΔE_p value was obtained compared to either the GCE/CoTAPc and GCE/AuNPs. This might be due to the arrangement of the two nanomaterials on the surface when combined. The AuNPs being added first, followed by the layer of the CoTAPc might have resulted in limited interaction of the AuNPs with the electrolyte to actually have an impact on the electrode electron transfer properties. Furthermore, passivation of the electrode is a possibility when now adding the CoTAPc layer on top of the GCE/AuNPs surface to form GCE/AuNPs/CoTAPc.

3.2.2. Electrochemical impedance spectroscopy (EIS)

EIS is well known as an effective tool for studying the properties of surface modified electrodes [35,36]. EIS measurement was carried out for the various electrodes (**1**–**8**), Nyquist plots are shown in Fig. 5B, with the obtained R_{ct} values obtained listed in Table 1. The data obtained were fitted using an equivalent modified circuit. The key parameter used to differentiate and characterize the modified electrodes was the charge transfer resistance (R_{ct}), which increases with decrease in conductivity and vice versa. The obtained data for the EIS data were in agreement with that obtained in cyclic voltammetry: the surface with the lowest ΔEp had the lowest R_{ct} values, Table 1.

3.2.3. Surface area coverage

The competitiveness of the various nanomaterials where electrode modification is concerned was further demonstrated by calculating the active surface area coverage of each modified surface. The effective electrode surface area (A_{eff}) of the modified GCE was determined in 1 mM $K_3[Fe(CN)_6]$ by applying the Randles–Sevcik Equation:

$$i_p = \left(2.69 \times 10^5\right) n^{3/2} D^{1/2} C A_{eff} v^{1/2} \quad (1)$$

where i_p is the peak current, n is equal to the number of electrons transferred (n ~ 1) , D is the diffusion coefficient of the analyte in solution (7.6×10^{-6} cm^2s^{-1}) [37] and C is the solution concentration in (mol/cm^{-3}), A_{eff} is the effective surface area (obtained by using Fig. 6C) and v is the scan rate (V/s^{-1}). Peaks near 0.5 V for CoTAPc containing electrodes are due to $Co^{III}Pc/Co^{II}Pc$ oxidation process in comparison with literature [38]. Ce nanoparticles are known to show cyclic voltammetry peaks around 0.3 V [39] as observed in Fig. 6A. Peaks due to Au NPs are usually observed at about 1 V [40]. Fig. 6B shows the obtained voltammograms for the surface GCE/CeO_2NPs as an example, at different scan rates (10 mV/s– 100 mV/s). A linear plot of peak current against root of scan rate is shown in the Fig. 6C, with an R^2 value of 0.9968.

By using the effective area of the modified electrodes determined using Eqn. (1) and the total charge determined by integrating peaks in Fig. 6A (anodic peaks), and then by employing Eqn. (2) [41], surface

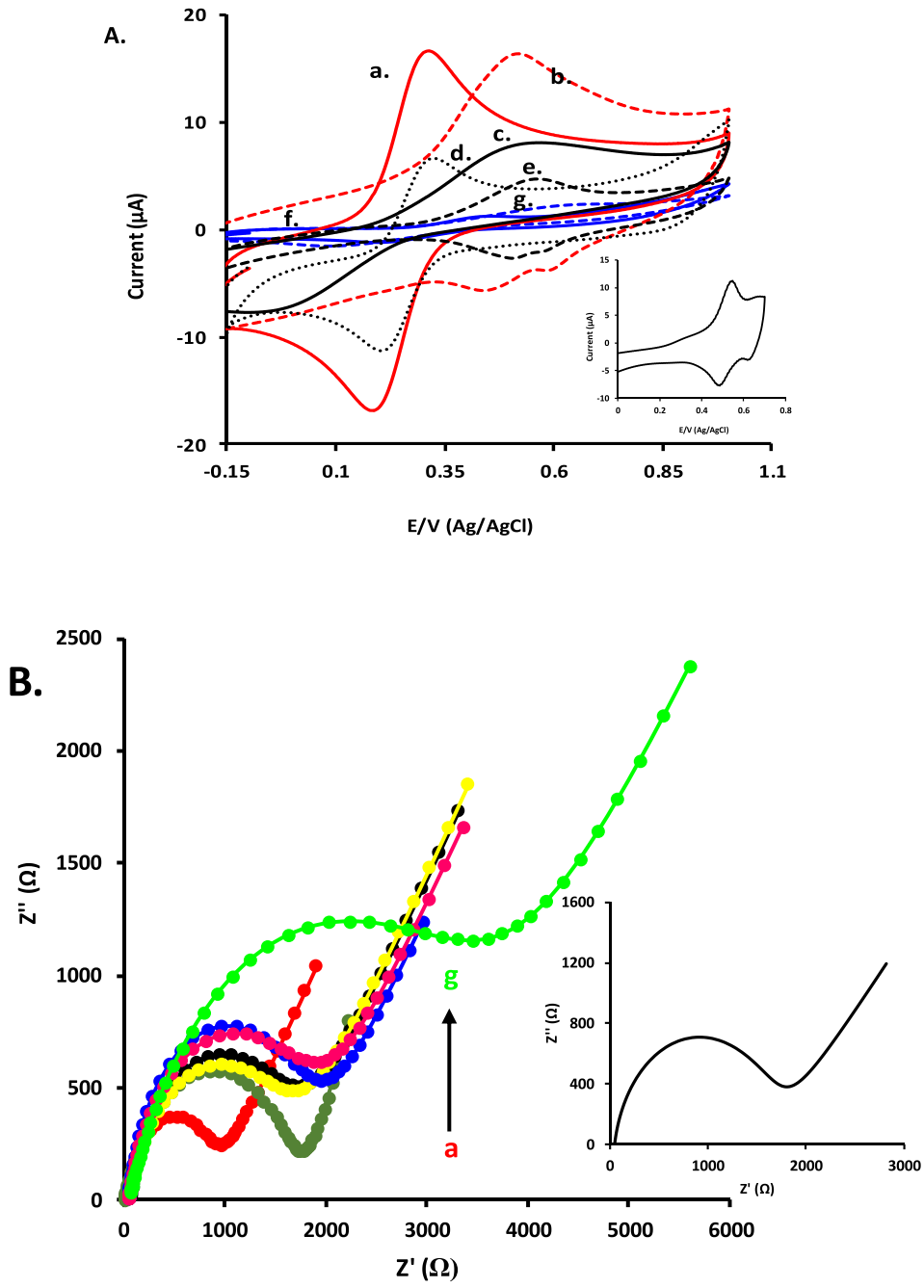

Fig. 5. CV (A) and EIS (B) data for GCE/CeO_2NPs_{COOH} (**3**) (a), GCE/CeO_2NPs_{COOH}/CoTAPc (seq.) (**7**) (b), GCE/SNGQDs(**2**) (c), GCE/SNGQDs(π)CoTAPc(**5**) (d), GCE/SNGQDs/CoTAPc (seq.)(**6**) (e), GCE/AuNPs (**4**) (f), GCE/AuNPs/CoTAPc (seq.) (**8**) (g). All in 1 mM $[FeCN_6]^{3-/4-}$ (in 0.1 M KCl) in 10 mM PBS. Scan rate = 100 mV/s. Insert: CV and EIS for GCE/CoTAPc(**1**).

coverages were calculated.

$$\Gamma = \frac{Q}{nFA_{eff}} \quad (2)$$

Where n is the number of electrons transferred (~1), F the Faraday constant (96.485C mol^{-1}), A is the effective surface area obtained from Eqn. (1) and Γ is the surface coverage. The higher surface coverages imply the increase in the electrode surface area which offers more electrocatalytic surface. The highest surface coverage was observed for GCE/AuNPs (**4**) (1.82×10^{-7} $mol.cm^{-2}$) compared to GCE/CeO_2NPs (**3**) (4.49×10^{-9} $mol.cm^{-2}$). The surface coverage obtained for the GCE/CoTAPc (1) was 1.11×10^{-14} $mol.cm^{-2}$. The Γ value for the GCE/SNGQDs was undetermined because no peak was observed. A peak was only observed upon incorporation with the CoTAPc. In the presence of CoTAPc, the highest surface coverage was obtained for the GCE/AuNPs/CoTAPc (**8**) (3.99×10^{-9} $mol.cm^{-2}$) compared to GCE/CeO_2NPs /CoTAPc (**7**) (2.65×10^{-10} $mol.cm^{-2}$), GCE/SNGQDs(π)CoTAPc(**5**) (1.49×10^{-13} $mol.cm^{-2}$) and GCE/SNGQDs/CoTAPc(seq) (**6**) (9.76×10^{-10} $mol.cm^{-2}$) surfaces. The highest surface coverage is for GCE/AuNPs (**4**) and the lowest is for GCE/CoTAPc (1).

3.3. HER2 detection

3.3.1. HER2 detection in PBS

The biorecognition of choice in this work is the HB5 aptamer. The used aptamer concentration (0.75 μM) is based on our previously

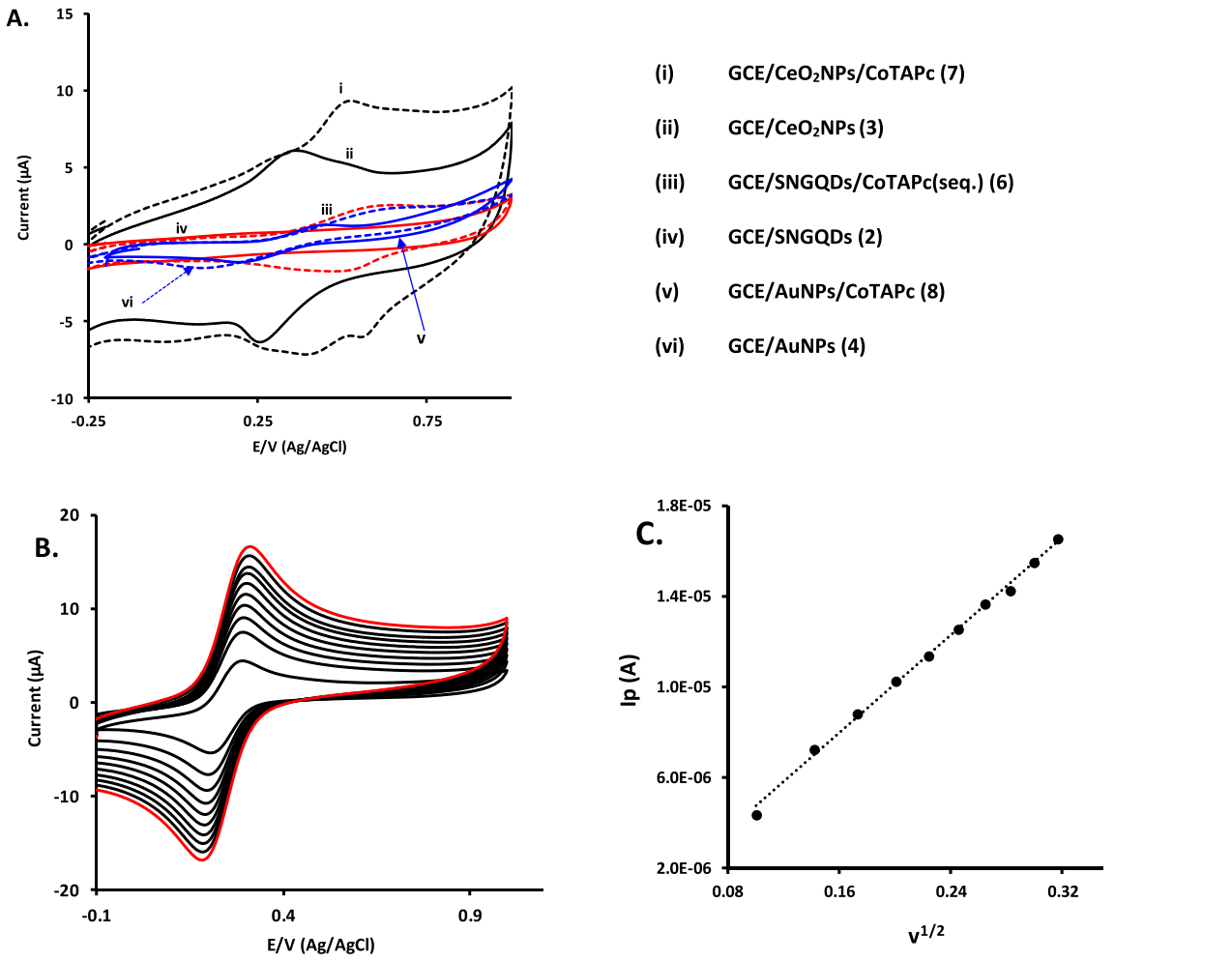

Fig. 6. A: Cyclic voltammograms of modified surfaces in 10 mM phosphate buffer solution of pH 7.4. Scan rate = 100 mV. s^{-1}. B: Effect of scan rates (10 mV/s −100 mV/s) obtained for the GCE/CeO_2NPs in 1 mM $[FeCN_6]^{3-/4-}$ (in 0.1 M KCl) in 10 mM PBS. Scan rate = 100 mV/s. C: Plot of peak current vs root of scan rate: $y = 5 \times 10^{-5}x - 7 \times 10^{-7}$, $R^2 = 0.9968$.

reported optimization data [21]. This concentration was used for all modified surfaces and the resulting electrodes were fabricated: CoTAPc (**1**)/HB5,

GCE/SNGQDs(**2**)/HB5, GCE/CeO_2NPs(**3**)/HB5, GCE/AuNPs(**4**)/HB5, GCE/SNGQDs(π)CoTAPc(**5**)/HB5, GCE/SNGQDs/CoTAPc(seq.)(**6**)/HB5, GCE/CeO_2NPs/CoTAPc(**7**)/HB5 and GCE/AuNPs/CoTAPc(**8**)/HB5. The resulting electrodes were all tested towards the electrochemical detection of HER2 at varying concentrations from 0 ng to 10 ng (which also represent the linear range), using the electrochemical impedance spectroscopy (EIS). Fig. 7 shows the Nyquist plots and corresponding regression plots obtained for the probes GCE/SNGQDs(**2**)/HB5 (Fig. 7A&B), GCE/CeO_2NPs(**3**)/HB5 (Fig. 7C&D), GCE/AuNPs(**4**)/HB5 (Fig. 7E&F) and GCE/AuNPs/CoTAPc (**8**)/HB5 (Fig. 7G&H) towards HER2 detection.

The figures clearly show that there was an increase in Rct with increase in HER2 concentration. This trend held true for all designed aptasensors, rest of the data shown in Fig. S2(A-H) (supporting information) and Table S1. Regression plots were then created using the data of each electrode, the equations of the regression plots were as follows:

(i) GCE/CoTAPc(**1**)/HB5:$y = 16901x - 3131.2, R^2 = 0.9698$
(ii) GCE/SNGQDs(**2**)/HB5:$y = 9650.4x - 5117.1, R^2 = 0.9233$
(iii) GCE/CeO_2NPs(**3**)/HB5:$y = 6001x + 1360.8, R^2 = 0.9878$
(iv) GCE/AuNPs(**4**)/HB5:$y = 43837x + 10461, R^2 = 0.9310$
(v) GCE/SNGQDs(π)CoTAPc(**5**)/HB5:$y = 11633x + 5513.6$, $R^2 = 0.9841$
(vi) GCE/SNGQDs/CoTAPc(seq.)(**6**)/HB5:$y = 6989.9x + 60.7, R^2 = 0.9645$
(vii) GCE/CeO_2NPs/CoTAPc(**7**)/HB5:$y = 24122x + 2780.6$, $R^2 = 0.9621$
(viii) GCE/AuNPs/CoTAPc(**8**)/HB5:$y = 13475x + 5479.7$, $R^2 = 0.9833$

The slopes (m) of the regression plots give the sensitivity of each sensor/modified electrode. The sensitivity of a biosensor is defined as the relationship between the change in analyte concentration and the intensity of the signal generated from the transducer [3]. Ideally, a biosensor should generate a signal in response to small fluctuations in the concentration of the target analyte. The sensitivity of a biosensor depends on various factors, and particularly for this work we observed and compared the role of three different nanoparticles: SNGQDs, CeO_2NPs and AuNPs towards enhancing electrochemical detection of HER2 on CoTAPc. Of the individual materials, the highest sensitivity was observed for AuNPs, followed by CoTAPc. We consider the structural characteristics of the various nanomaterials and the way in which they are distributed onto the electrode. Furthermore, we look at the way in which they interact with the HB5 as the recognition element for the HER2 antigen. We have earlier demonstrated that the GCE/AuNPs had higher surface coverage (1.82×10^{-7} mol.cm^{-2}). This may imply more HB5 fragments adsorbed on the electrode compared to the GCE/SNGQDs and GCE/CeO_2NPs modified surfaces, hence the higher and better sensitivity. The performance of CoTAPc in the presence of the

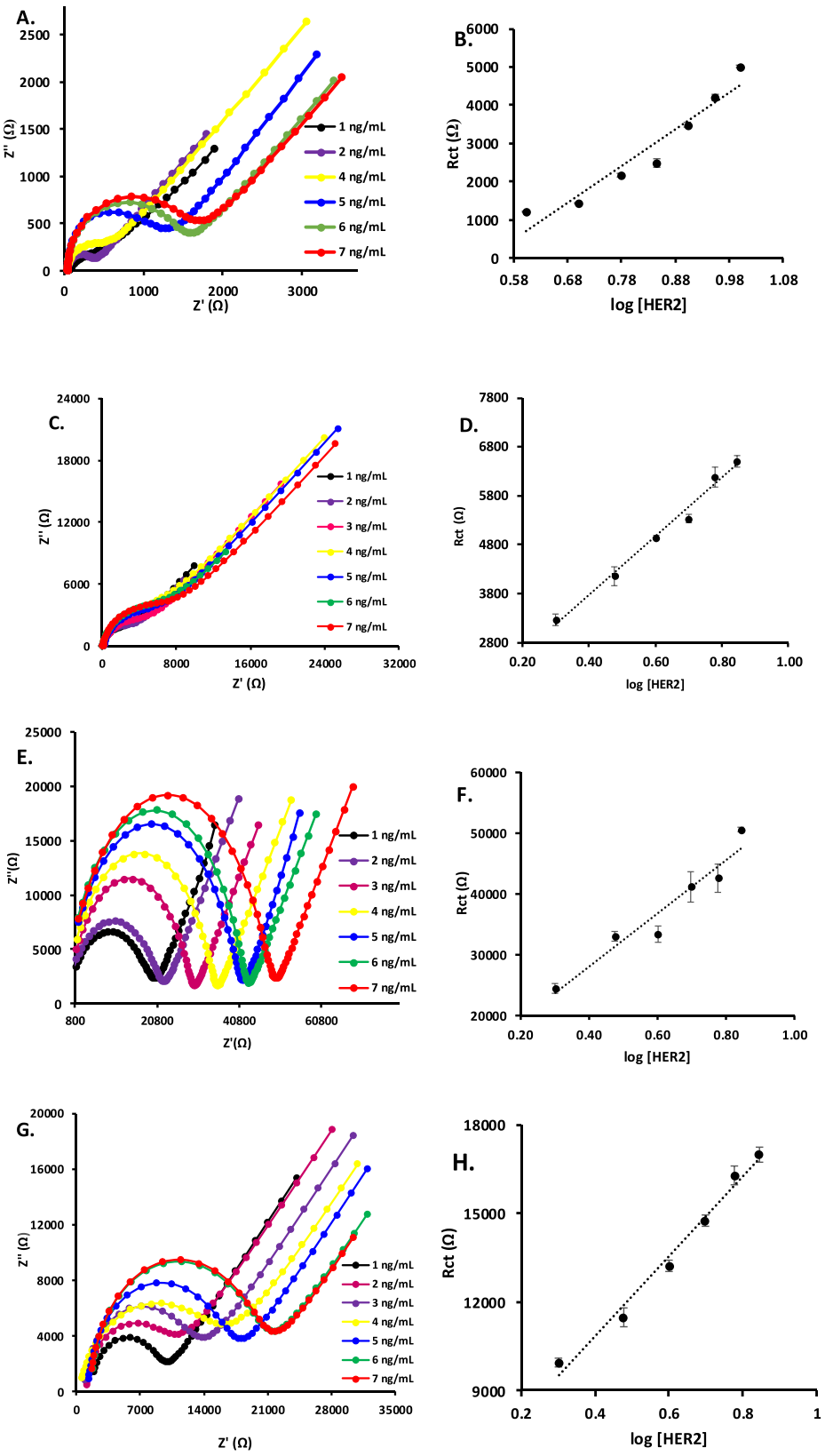

Fig. 7. Nyquist plots and regression plot of R_{ct} vs log [HER2] for the probes GCE/SNGQDs(**2**)/HB5 (A & B), GCE/CeO_2NPs(**3**) (C & D), GCE/AuNPs(**4**)/HB5 (E & F) and GCE/AuNPs/CoTAPc(**8**)/HB5 (G & F) as labelled. All in $Fe(CN)_6]^{3-/4-}$ (1 mM in 0.1 $mol\cdot^{L-1}$ KCl in 10 mM PBS (pH 7.4).

three nanoparticles will now be discussed. The CoTAPc on its own functions as an immobilization platform for the HB5 aptamer, as well as signal amplification owing to its redox and electrocatalytic properties. Varying effects on the sensitivities for all electrodes when the nanoparticles are combined with the CoTAPc for sensor fabrication were observed.

In the presence of CoTAPc, GCE/CeO_2NPs/CoTAPc(**7**)/HB5 showed the highest sensitivity value (24122 Ωng^{-1}mL) compared to GCE/SNGQDs/CoTAPc(seq.)(**6**)/HB5 (6990 Ωng^{-1}mL), GCE/AuNPs/CoTAPc (**8**)/HB5 (13475 Ωng^{-1}mL), and GCE/SNGQDs(π)CoTAPc(**5**)/HB5 (11633 Ωng^{-1}mL). Table 2 shows that the NPs reduce the sensitivity of CoTAPc with the exception of CeO_2 NPs. Based on the results, a much more stable sensing platform for HB5 immobilization, and in turn signal amplification for HER2 detection was developed for the GCE/CeO_2NPs/CoTAPc(**7**)/HB5 aptasensor.

The effect of the sp^2 hybridized characteristic of the SNGQDs in π-π interactions with the CoTAPc was demonstrated in the obtained results. A higher sensitivity was obtained for GCE/SNGQDs(π)CoTAPc(**5**)/HB5 (11633 Ωng^{-1}mL) compared to the sequentially modified surface GCE/SNGQDs/CoTAPc(seq.)(**6**)/HB5 (6990 Ωng^{-1}mL), showing the advantage of non-covalent arrangement when compared to sequentially modified electrode. There was no general trend amongst all electrodes where the sensitivity is concerned. This speaks to the peculiarity of each nanoparticle structure, their interaction with the CoTAPc, physicochemical properties and in turn their electrochemical behaviour. The obtained results solidify the peculiar and comparative nature of each nanoparticle: SNGQDs, CeO_2NPs and AuNPs, and in turn their electrochemical activity as either signal amplifiers or immobilization platforms . The linearity of the e data obtained for each aptasensor can be characterized using the R^2 value for each regression plot. The R^2 value obtained shows the accuracy of the measured response. The best linearity was obtained for the probes: GCE/CeO_2NPs(**3**)/HB5, GCE/SNGQDs(π)CoTAPc(**5**)/HB5 and GCE/AuNPs/CoTAPc(**8**)/HB5, all with $R^2 > 0.98$ (equations (iii) – (iv)) above.

The limit of detection (LOD) values for all ten probes were estimated by the equation 3σ/*s*. In which σ is the standard deviation of R_{ct} values obtained for PBS (without HER2) respectively for all probes, and *s* is the sensitivity and slope of the regression plots. The list of the modified surfaces with their obtained LOD values is shown in Table 2. The best LOD value was obtained for the probe, GCE/AuNPs(**4**)/HB5 0.006 ng/mL, and the highest LOD value was obtained for the probe GCE/SNGQDs (**2**)/HB5 0.29 ng/mL. The LOD of CoTAPc improved in the presence CeO_2NPs corresponding the improvement in sensitivity. A lower LOD was obtained for GCE/SNGQDs(π)CoTAPc(**5**)/HB5 (0.074 ng/mL) compared to the sequentially modified surface GCE/SNGQDs/CoTAPc (seq.)(**6**)/HB5 (0.19 ng/mL).

The LOD values reported in this work were found to be comparable (and sometimes better) to the ones reported in literature on aptamer based detection of HER2 [42–50], Table 3. This demonstrates potential applicability of the designed sensors for HER2 biosensor design.

Table 2
Limit of detection (LOD) and sensitivities for detection of HER2 biosensors developed in this work. Linear range 1–10 ng/mL in all cases.

Electrodes [a]	Sensitivity (Ωng^{-1}mL)	LOD (ng/mL)
GCE/CoTAPc(**1**)/HB5	16,901	0.051
GCE/SNGQDs(**2**)/HB5	9650	0.29
GCE/CeO_2NPs(**3**)/HB5	6001	0.19
GCE/AuNPs(**4**)/HB5	43,837	0.006
GCE/SNGQDs(π)CoTAP(**5**)/HB5	11,633	0.074
GCE/SNGQDs/CoTAPc(seq.)(**6**)/HB5	6990	0.19
GCE/CeO_2NPs/CoTAPc(**7**)/HB5	24,122	0.008
GCE/AuNPs/CoTAP(**8**)/HB5	13,475	0.058

[a] Electrode numbers in brackets.

Table 3
Comparison of the data reported in literature for impedimetric HER2 biosensors with biosensor developed in this work. EIS employed in all cases.

Modified Electrodes	Linear Range (ng/mL)	LOD (ng/mL)	References
AuNPs Electrode	$10^{-5} - 10^{2}$	5	42
Gold Electrode-MnFePBA@AuNPs	0.001–1.0	0.000247	43
AuNPs/MW-CILE	10–110	7.4	44
SPCE-AuNPs	0.01–100	0.01	45
Thiolated DNA aptamer-Au	$0.1 - 10^{4}$	0.1	46
GE/rGONs/Rh-NPs/aptamer/HER2-ECD	10–500	0.665	47
SPCE)/CdSe@ZnS Quantum Dots (QDs)	10–150	2.1	48
SPCE/MBs	5–50 and 50–500	2.8	49
MCH/Af/AuNPs/GSPE	$0–4 \times 10^{4}$	6×10^{3}	50
GCE/CoTAPc(**1**)/HB5	1–10	0.051	This work
GCE/SNGQDs(**2**)/HB5	1–10	0.29	This work
GCE/CeO_2NPs(**3**)/HB5	1–10	0.19	This work
GCE/AuNPs(**4**)/HB5	1–10	0.006	This work
GCE/SNGQDs(π)CoTAPc(**5**)/HB5	1–10	0.074	This work
GCE/SNGQDs/CoTAPc(seq.)(**6**)/HB5	1–10	0.19	This work
GCE/CeO_2NPs/CoTAPc(**7**)/HB5	1–10	0.008	This work
GCE/AuNPs/CoTAPc(**8**)/HB5	1–10	0.058	This work

AuNPs = Gold nanoparticles, MnFePBA = Bimetallic Manganese Iron Perussian Blue Analogue, Rh-NPs = Rhodium nanoparticles, ECD = Extracellular domain, MB = Magnetic Beads, rGONs = Reduced Graphene Nanosheets, MCH = 6-mercapto-1-hexanol, Af = Affibody, GSPE = Graphite Screen Printed Electrode, MW-CILE = Multiwalled Carbon Nanotube Ionic Liquid Electrode and GCE = Glassy Carbon Electrode.

3.3.2. *Repeatability and stability*

The stability of the listed probes above, was determined using the shelf-life estimation method. [HER2] = 5 ng/mL in 10 Mm PBS (pH 7.4) was employed in all cases. The probes were stored at 4 °C. After every 24-h period, the stability of the sensor probes was investigated by running electrochemical impedance spectroscopy (EIS) and measuring the R_{ct} values in 1 mM $Fe(CN)_6]^{3-/4-}$ in 0.1 mol·L^{-1} KCl in 10 mM PBS (pH 7.4). The stability of each surface was assessed by looking at the change in the R_{ct} values from the first 24 h up until the 96 h, and was characterized by using the relative standard deviation (RSD) of the daily obtained R_{ct} values, Fig. 8A. 96 h was employed since it has been reported to be adequate time to assess the shelf-life of a sensor [51]. Each measurement was made in triplicate daily for each probe, up until the fourth day. The stability of the selected probes over the 96 h period was in the following trend (% RSD): GCE/SNGQDs(**2**)/HB5/HER2 (1.22 %) > GCE/AuNPs(**4**)/HB5/HER2 (2.32 %) > GCE/CeO_2NPs(**3**)/HB5/HER2 (5.54 %). An improved stability was observed for the GCE/AuNPs(**4**)/HB5/HER2 when the CoTAPc was incorporated forming the probe; GCE/AuNPs/CoTAPc(**8**)/HB5/HER2 (0.56 %). This result emphasizes the significance of combining nanostructures for desirable and improved sensing characteristics. All electrodes in question showed fair stability towards HER2 over the 96 h period, with acceptable deviation for biosensors.

The repeatability of the designed aptasensors is demonstrated throughout, the experiments were run (n = 3) at all concentrations for all ten electrodes, Table S1. The relative standard deviation (RSD) for all ten electrodes at various concentrations was determined, acceptable values for biosensor designed were obtained. Fig. 8B shows the repeatability of the results obtained for all electrodes at HER2 = 5 ng/mL in terms of % RSD for n = 3 cycles for each electrode.

3.3.3. *HER2 detection in human serum*

The accuracy of the method was tested, by spiking serum samples from normal human with different concentrations of HER2. The serum was diluted 500-fold. The specificity of the various probes was

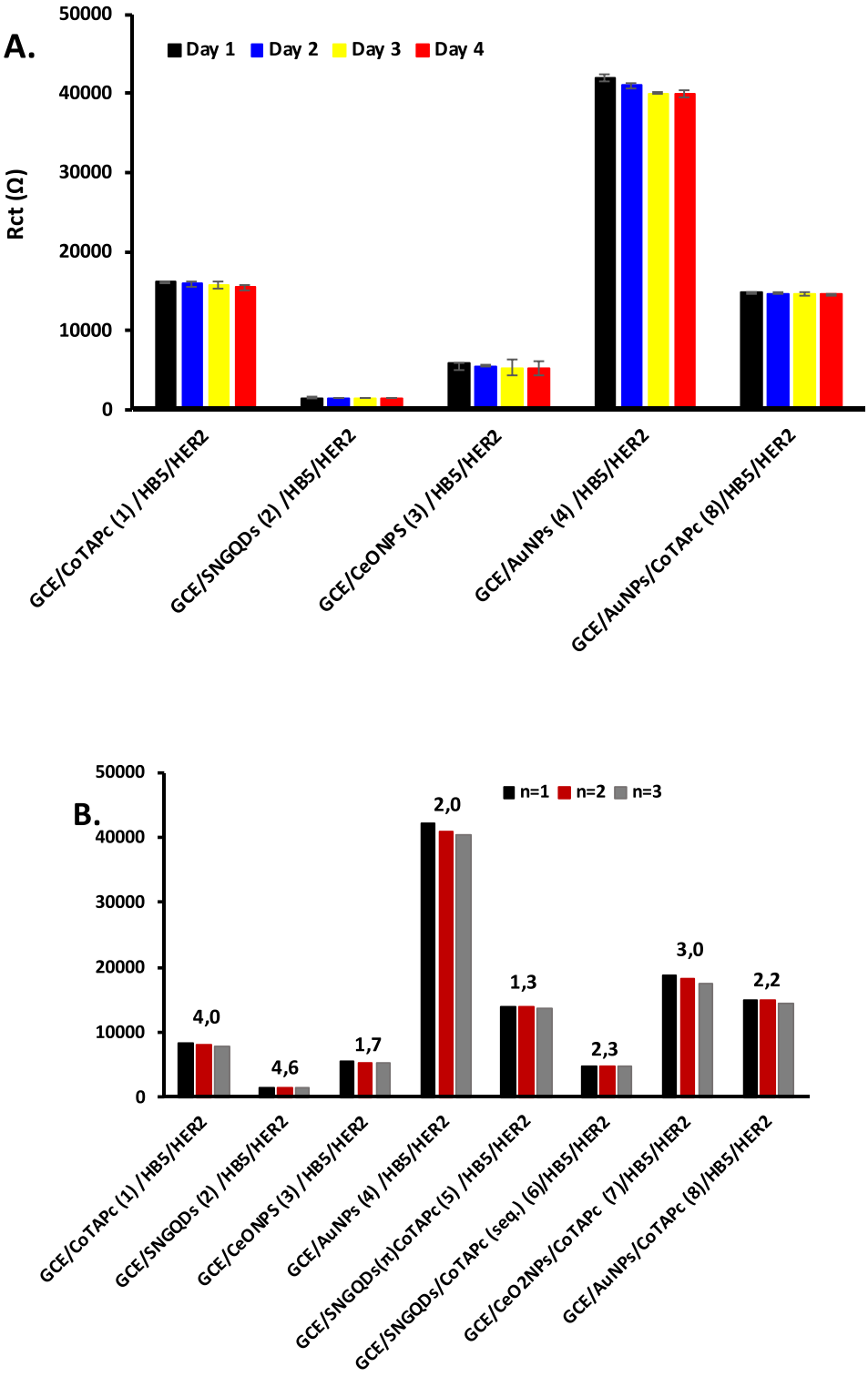

Fig. 8. A: Storage stability assessment of selected probes upon interaction with HER2 ([HER2] = 5 ng/mL, n = 3), and B: Repeatability of all the designed probes at ([HER2] = 5 ng/mL, n = 3: overall % RSD values are shown above bars for n = 1–3) for each electrode. All in $Fe(CN)_6]^{3-/4-}$ (1 mM in 0.1 mol·L − 1 KCl in 10 mM PBS (pH 7.4).

investigated in terms of percentage recoveries at four concentrations 1 ng/mL, 3 ng/mL, 5 ng/mL and 7 ng/mL. The different probes were then tested on their ability to detect or recover HER2, in the competitive human serum environment. Table 4, shows results obtained for the best performing probes: GCE/AuNPs/CoTAPc(**8**)/HB5 and GCE/SNGQDs/CoTAPc(seq.)(**6**)/HB5 for HER2 detection in human serum. The data obtained for the rest of the electrodes is shown in Table S2 (supporting information). The following % recoveries were obtained for the electrodes containing single nanostructures: GCE/CoTAPc(**1**) /HB5 (43 % – 65 %), GCE/SNGQDs(**2**)/HB5 (31 % – 120 %), GCE/CeO_2NPs(**3**)/HB5 (50 % – 103 %) and GCE/AuNPs(**4**)/HB5 (63 % – 120 %). The recoveries were less than 80 % in some cases, and this could be due matrix effect [52]. An improvement was observed for CoTAPc in the presence of each of the nanoparticles (CeO_2NPs or SNGQDs or AuNPs). The best %

Table 4
Table of % recovery of HER2 in human serum for the probes GCE/AuNPs/CoTAPc(**8**)/HB5 (i) and GCE/SNGQDs/CoTAPc(seq.)(**6**)/HB5 (ii) as examples. RSD = relative standard deviation. SDEV = standard deviation.

(i)							
[HER2] added ng/mL	R_{ct} 1 (Ω)	R_{ct} 2 (Ω)	R_{ct} 3 (Ω)	Average	SDEV	% RSD	%Recovered
1	8400	8100	8000	8167	208	2.55	120
3	19,200	19,300	19,700	19,400	265	1.36	93
5	25,300	25,600	25,000	25,300	300	1.19	86
7	30,900	30,400	30,000	30,433	451	1.48	91
(ii)							
[HER2] added ng/mL	R_{ct} 1 (Ω)	R_{ct} 2 (Ω)	R_{ct} 3 (Ω)	Average	SDEV	% RSD	%Recovered
1	1320	1300	1290	1303	12	0.96	119
3	4010	3950	3910	3957	41	1.04	58
5	9740	9750	9970	9820	106	1.08	81
7	14,800	14,700	15,300	14,933	262	1.76	93

recoveries was obtained for GCE/AuNPs/CoTAPc(**8**)/HB5 (86 % – 120 %). The sequentially modified surface GCE/SNGQDs/CoTAPc(seq.)(**6**)/HB5 had better % recoveries (81 % – 119 %) compared to its counter GCE/SNGQDs(π)CoTAPc(**5**)/HB5 (63 % – 114 %). The results obtained show the feasibility and potential of the aptasensors: GCE/AuNPs/CoTAPc(**8**)/HB5 and GCE/SNGQDs/CoTAPc(seq.)(**6**)/HB5 for real life application of the detection of HER2 in early breast cancer diagnosis in human serum.

4. Conclusions

This work investigates the applicability of a cobalt tetra phenoxy acetic acid phthalocyanine (CoTAPc), as an immobilization platform for the HB5 aptamer as well as signal amplification towards the detection of HER2. In an attempt to improve the efficiency of the CoTAPc as an electrode modifier for biosensor design, it was coupled with three nanoparticles; AuNPs, SNGQDs and CeO_2NP_s. The highest sensitivity and lowest LOD values were obtained for the GCE/AuNPs (**4**)/HB5. The combination of the respective nanoparticles with the CoTAPc on the electrode surface was achieved by sequential adsorption as well as, π-π stacking for SNGQDs. A higher sensitivity and low LOD value was obtained for the probe GCE/SNGQDs(π)CoTAPc (**5**)/HB5, compared to the sequentially modified GCE/SNGQDs/CoTAPc(seq.) (**6**)/HB5. This result demonstrates the effect of spatial arrangement and interactions of the nanomaterials on the electrode in biosensor design. The highest storage stability was observed for the GCE/AuNPs/CoTAPc (**8**)/HB5 aptasensor. The sensors showed great reproducibility and sensitivity towards the detection of HER2. The functionality and real life applications of the sensors was investigated in human serum samples containing known HER2 amounts. The sensors showed excellent results in HER2 detection in human serum sample. The results obtained, show the potential of combining cobalt based phthalocyanines with various nanomaterials for biosensor design towards HER2 detection. The sensors showed sensitivity towards the HER2 protein and have considerable potential as an effective alternative method for the early detection of HER2.

Declaration of Competing Interest

The authors declare that they have no known competing financial interests or personal relationships that could have appeared to influence the work reported in this paper.

Data availability

Data will be made available on request.

Acknowledgements

This work was supported by the Department of Science and Innovation (DSI) and National Research Foundation through DSI/NRF South African Research Chairs Initiative for Professor of Medicinal Chemistry and Nanotechnology (UID 62620), Rhodes University, and DSI/Mintek Nanotechnology Innovation Center-Sensors.

Appendix A. Supplementary material

Supplementary data to this article can be found online at https://doi.org/10.1016/j.bioelechem.2022.108301.

References

[1] D. Grieshaber, R. MacKenzie, J. Vörös, E. Reimhult, Electrochemical biosensors - sensor principles and architectures, Sensors 8 (2008) 1400–1458.
[2] C, Tortolini, G, Sanzò, R, Antiochia, F, Mazzei and G, Favero, Application of a nanostructured enzymatic biosensor based on fullerene and gold nanoparticles to polyphenol detection, In: Prickril B., Rasooly A, (eds) Biosensors and Biodetection. Methods in Molecular Biology, Humana Press, New York, NY. 1572 (2017) 41-53 https://doi.org/10.1007/978-1-4939-6911-1_4 .
[3] N. Bhalla, P. Jolly, N. Formisano, P. Estrela, Introduction to biosensors, Essays Biochem. 60 (2016) 1–8.
[4] B. Prieto-Simón, M. Campàs, J.L. Marty, Biomolecule immobilization in biosensor development: tailored strategies based on affinity interactions, Protein. Pept. Lett. 15 (2008) 757–763.
[5] V. Naresh, N. Lee, A Review on biosensors and recent development of nanostructured materials-enabled biosensors, Sensors 21 (2021) 1109, https://doi.org/10.3390/s21041109.
[6] W. Tai, R. Mahato, K. Cheng, The role of her2 in cancer therapy and targeted drug delivery, J. Control Release 146 (2010) 264–275.
[7] N. Iqbal, N. Iqbal, Human epidermal growth factor receptor 2 (HER2) in cancers: overexpression and therapeutic implications, Mol. Biol. Int. 2014 (2014) 1–9.
[8] A.M. Schmidt, M.J.F. Calvete, Phthalocyanines: an old dog can still have new (photo)tricks, Molecules 26 (2021) 2823, https://doi.org/10.3390/molecules26092823.
[9] C. Stefanov, J.(.F. van Staden, R.-I. Stefan-van Staden, Review—Enzymatic and non-enzymatic (bio)sensors based on phthalocyanines: a minireview. ECS J. Solid State, Sci. Technol. 9 (5) (2020) 051012.
[10] T, Nyokong, N4-macrocyclic metal complexes: electrocatalysis, electrophotochemistry, and biomimetic electrocatalysis. J.H. Zagal, F. Bedioui, J.-P. Dodelet (Eds.), Springer (2006) Chpt. 7 ISBN0-387-28429.
[11] M. E, Hamdy, M. D, Carlo, H. A, Hussein, T. A, Salah, A. H, El–Deeb, M. M, Emara, G, Pezzoni and D, Compagnone, Development of gold nanoparticles biosensor for ultrasensitive diagnosis of foot and mouth disease virus. J. Nanobiotechnology. 16 (2018) 48 .
[12] J.M. Pingarrón, P. Yanez-Sedeno, A. Gonzalez-Cortes, Gold nanoparticle-based electrochemical biosensors, Electrochim. Acta 53 (2008) 5848–5866.
[13] Y. Shao, J. Wang, H. Wu, J. Liu, I. Aksay, Y. Lin, Graphene based electrochemical sensors and biosensors: a review, Electroanalysis 22 (10) (2010) 1027–1036.
[14] S. Bag, C. Raj, On the electrocatalytic activity of nitrogen-doped reduced graphene Oxide: Does the nature of nitrogen really control the activity towards oxygen reduction, J. Chem. Sci. 128 (2016) 339–347.
[15] A.S. Karakoti, P. Munusamy, K. Hostetler, V. Kodali, S. Kuchibhatla, G. Orr, J. G. Pounds, J.G. Teeguarden, B.D. Thrall, D.R. Baer, Preparation and characterization challenges to understanding environmental and biological impacts of ceria nanoparticles, Surf. Interface Anal. 44 (2012) 882–889.
[16] H. Liying, S. Yumin, J. Lanhong, S. Shikao, Recent advances of cerium oxide nanoparticles in synthesis, luminescence and biomedical studies: A review, J. Rare Earths 33 (2017) 791–799.

[17] C. Xu, X. Qu, Cerium oxide nanoparticle: a remarkably versatile rare earth nanomaterial for biological applications, NPG Asia Materials 60 (2014), https://doi.org/10.1038/am.2013.88.
[18] S.R. Nxele, R. Nkhahle, T. Nyokong, The synergistic effects of coupling Au nanoparticles with an alkynyl Co(II) phthalocyanine on the detection of prostate specific antigen, Talanta 237 (2022), 122948, https://doi.org/10.1016/j.talanta.2021.122948.
[19] S. Centane, T. Nyokong, The antibody assisted detection of HER2 on a cobalt porphyrin binuclear framework and gold functionalized graphene quantum dots modified electrode, J. Electroanal. Chem. 880 (2021), 114908, https://doi.org/10.1016/j.jelechem.2020.114908.
[20] S. Centane, T. Nyokong, Impedimetric aptasensor for her2 biomarker using graphene quantum dots, polypyrrole and cobalt phthalocyanine modified electrodes, Sens. Bio-Sens. Res 34 (2021) 100467.
[21] S. Centane, S. Mgidlana, Y. Openda, T. Nyokong, Electrochemical detection of human epidermal growth factor receptor 2 using an aptamer on cobalt phthalocyanines - cerium oxide nanoparticle conjugate, Bioelectrochemistry 146 (2022), 108146, https://doi.org/10.1016/j.bioelechem.2022.108146.
[22] L. Polavarapu, N. Venkatram, W. Ji, Q.-H. Xu, Optical-limiting properties of oleylamine-capped gold nanoparticles for both femtosecond and nanosecond laser pulses, ACS Appl. Mater. Interfaces 1 (10) (2009) 2298–2303.
[23] O.J. Achadu, T. Nyokong, Interaction of graphene quantum dots with 4-acetamido-2,2,6,6-tetramethylpiperidine-oxyl free radicals: a spectroscopic and fluorimetric study, J. Flouresc. 26 (2016) 283–295.
[24] A. Maringa, E. Antunes, T. Nyokong, Electrochemical behaviour of gold nanoparticles and Co tetraaminophthalocyanine on glassy carbon electrode, Electrochim. Acta 121 (2014) 93–101.
[25] A. Samanta, Z. Deng, Y. Liu, H. Yan, A perspective on functionalizing colloidal quantum dots with DNA, Nano Res. 6 (2013) 853–858.
[26] Q. Fan, K. Liu, Z. Liu, H. Liu, L. Zhang, P. Zhong, C. Gao, A ligand-exchange route to nobel metal nanocrystals with a clean surface for enhanced optical and catalytic properties, Part. Part. Syst. Charact. 34 (2017) 1700075, https://doi.org/10.1002/ppsc.201700075.
[27] L. Lu, S. Zou, B. Fang, The critical impacts of ligands on heterogeneous nanocatalysis: a review, ACS Catal. 11 (10) (2021) 6020–6058.
[28] A. Filtschew, K. Hofmann, C. Hess, Ceria and its defect structure: new insights from a combined spectroscopic approach, J. Phys. Chem. C 120 (2016) 6694–6703.
[29] C. Schilling, A. Hofmann, C. Hess, M.V. Ganduglia-Pirovano, Raman spectra of polycrystalline CeO_2: a density functional theory study, J. Phys. Chem. C 121 (2017) 20834–20849.
[30] J. Cui, G.A. Hope, Raman and fluorescence spectroscopy of CeO_2, Er_2O_3, Nd_2O_3, Tm_2O_3, Yb_2O_3, La_2O_3, and Tb_4O_7, J. Spectrosc. (Hindawi) 2015 (2015) 1–8.
[31] R, Zamiri, H. A, Ahangar, A, Kaushal, A, Zakaria, G, Zamiri, D, Tobaldi and J. M. F, Ferreira, Dielectrical properties of CeO_2 nanoparticles at different temperatures. PLoS ONE 10 (2017) e0122989 http://doi:10.1371/journal.pone.0122989.
[32] M. He, B. Cao, X. Gao, B. Liu, J. Yang, Synthesis of multi-branched gold nanostructures and their surface-enhanced raman scattering properties of 4-aminothiophenol, J. Mate. Res. 34 (2019) 2928–2934.
[33] L.C. Mecker, K.M. Tyner, J.F. Kauffman, S. Arzhantsev, D.J. Mans, C. M. Gryniewicz-Ruzicka, Selective melamine detection in multiple sample matrices with a portable raman instrument using surface enhanced raman spectroscopy-active gold nanoparticles, Anal. Chim. Acta 733 (2012) 48–55.
[34] S. Saddeler, U. Hagemann, S. Schulz, Effect of the size and shape on the electrocatalytic activity of Co_3O_4 nanoparticles in the oxygen evolution reaction, Inorg. Chem. 59 (2020) 10013–10024.
[35] B.-Y. Chang, S.-M. Park, Electrochemical impedance spectroscopy, Annu. Rev. Anal. Chem. 3 (1) (2010) 207–229.
[36] S. Wang, J. Zhang, O. Gharbi, V. Vivier, M. Gao, M.E. Orazem, Electrochemical impedance spectroscopy, Nat. Rev. Methods Primers 1 (2021) 41, https://doi.org/10.1038/s43586-021-00039-w.
[37] J.J. Gooding, V.G. Praig, E.A. Hall, Platinum-catalyzed enzyme electrodes immobilized on gold using self-assembled layers, Anal. Chem. 70 (1998) 2396–2402.
[38] C.A. Caro, F. Bedioui, J.H. Zagal, Electrocatalytic oxidation of nitrite on a vitreous carbon electrode modified with cobalt phthalocyanine, Electrochim. Acta. 47 (2002) 1489–1494.
[39] T. Saravanan, M. Shanmugam, P. Anandan, M. Azhagurajan, K. Pazhanivel, M. Arivanandhan, Y. Hayakawa, R. Jayavel, Facile synthesis of graphene-ceo2 nanocomposites with enhanced electrochemical properties for supercapacitors, Dalton Trans. 44 (2015) 9901–9908.
[40] T. Hezard, K. Fajerwerg, D. Evrard, V. Collière, P. Behra, P. Gros, Gold nanoparticles electrodeposited on glassy carbon using cyclic voltammetry: application to hg(ii) trace analysis, J. Electroanal. Chem. 664 (2012) 46–52.
[41] C.W. Foster, J. Pillay, J.P. Metters, C.E. Banks, Cobalt phthalocyanine modified electrodes utilised in electroanalysis: nano-structured modified electrodes vs. bulk modified screen-printed electrodes, Sensors 14 (2014) 21905–21922.
[42] L. Chuna, S. Kima, M. Cho, W. Choe, J. Nam, D.W. Lee, Y. Lee, Electrochemical detection of HER2 using single stranded DNA aptamer modified gold nanoparticles electrode, Sensors Actua. B Chem. 186 (2013) 446–450.
[43] N. Zhou, F. Su, Z. Li, X. Yan, C. Zhang, B. Hu, L. He, M. Wang, Z. Zhang, Gold nanoparticles conjugated to bimetallic manganese(ii) and iron(ii) prussian blue analogues for aptamer-based impedimetric determination of the human epidermal growth factor receptor-2 and living MCF-7 cells, Microchim. Acta. 75 (2019), https://doi.org/10.1007/s00604-018-3184-9.
[44] E. Arkan, R. Saber, Z. Karimi, M. Shamsipur, A novel antibody–antigen based impedimetric immunosensor for low level detection of HER2 in serum samples of breast cancer patients via modification of a gold nanoparticles decorated multiwall carbon nanotube-ionic liquid electrode, Analyt. Chim. Acta 874 (2015) 66–74.
[45] S. Sharma, J. Zapatero-Rodríguez, R. Saxena, R. O'Kennedy, S. Srivastava, Ultrasensitive direct impedimetric immunosensor for detection of serum HER2, Biosens. Bioelectron. 106 (2018) 78–8579.
[46] S.K. Arya, P. Zhurauski, P. Jolly, M.R. Batistuti, M. Mulato, P. Estrela, Capacitive aptasensor based on interdigitated electrode for breast cancer detection in undiluted human serum, Biosens. Bioelectron. 102 (2018) 106–112.
[47] M. Sadeghi, S. Kashanian, S.M. Naghib, E. Arkan, A high-performance electrochemical aptasensor based on graphene-decorated rhodium nanoparticles to detect HER2-ECD oncomarker in liquid biopsy, Sci. Rep 12 (2022) 3299, https://doi.org/10.1038/s41598-022-07230-3.
[48] M, Freitas, M, M.P.S Neves, H. P. A, Nouws and C, Delerue-Matos, Quantum dots as nanolabels for breast cancer biomarker HER2-ECD analysis in human serum. Talanta 208 (2020) 120430 https://doi.org/10.1016/j.talanta.2019.120430 .
[49] M. Freitas, H.P.A. Nouws, E. Keating, C. Delerue-Matos, High-performance electrochemical immunomagnetic assay for breast cancer analysis, Sens. Actuators B Chem. 308 (2020), 127667, https://doi.org/10.1016/j.snb.2020.127667.
[50] A. Ravalli, C. Gomes da Rocha, H. Yamanaka, G. Marrazza, A label-free electrochemical affisensor for cancer marker detection: the case of HER2, Bioelectrochemistry 106 (2015) 268–275.
[51] P. Panjan, V. Virtanen, A.M. Sesay, Determination of stability characteristics for electrochemical biosensors via thermally accelerated ageing, Talanta 170 (2017) 331–336.
[52] Y. Rosenberg-Hasson, L. Hansmann, M. Liedtke, I. Herschmann, H.T. Maecker, Effects of serum and plasma matrices on multiplex immunoassays, Immunol. Res. 58 (2014) 224–233.